Room temperature NO2 gas sensor based on stain-etched porous silicon: Towards a low-cost gas sensor integrated on silicon

H. Mhamdi, K. Azaiez, T. Fiorido, R. Benabderrahmane Zaghouani, J.L. Lazzari, Marc Bendahan, W. Dimassi

Room temperature NO_2 gas sensor based on stain-etched porous silicon: towards a low-cost gas sensor integrated on silicon

H. Mhamdi[1,5], K. Azaiez[2] , T. Fiorido[3], R. Benabderrahmane Zaghouani[1*], J. L. Lazzari[4], M. Bendahan[3], W. Dimassi[2]

[1]*Laboratoire de Photovoltaïque, Centre de Recherches et des Technologies de l'Energie, Technopôle de Borj-Cédria, BP, 95 Hammam-Lif, Tunis, Tunisie*

[2]*Laboratoire de Nanomatériaux et Systèmes pour Energies Renouvelables, Centre de Recherches et des Technologies de l'Energie, Technopôle de Borj-Cédria, BP, 95 Hammam-Lif, Tunis, Tunisie*

[3] *Aix Marseille Univ, Université de Toulon, CNRS, IM2NP, Marseille, France*

[4]*Aix Marseille Université, CNRS, CINaM UMR 7325,*

Campus de Luminy, Case 913, 163, Avenue de Luminy, 13288 Marseille Cedex 09, France

[5]*Faculté des Sciences Mathématiques, Physiques et Naturelles de Tunis*

[*]Corresponding author: Rabia Benabderrahmane

Tel.:+216 96148416; Fax: +216 79325825

E-mail address: rabia.benabderrahmane@gmail.com

Abstract

In this work, we investigate the use of a new low-cost gas sensor based on porous silicon to detect low concentration of NO_2 at room temperature. In this work, we focused on the gas sensing properties of two different types of porous silicon (PS) prepared by a simple chemical method namely nano-porous silicon (nano-PS) and macro-porous silicon (macro-PS). The prepared sensors are characterized by different pores size, thicknesses and porosity. Electronic properties of the synthesized structures were studied by measuring the effective minority carrier lifetime using a µPCD lifetime tester. Structural properties and morphology of PS samples were also presented using Fourier transforms infrared (FTIR) spectroscopy and scanning electron microscope (SEM). The gas sensing properties of nano-PS and macro-PS were performed at room temperature for NO_2 gas. Macro-PS and nano-PS sensors exhibit different behaviors attributed to the difference in their morphologies. The tested sensors exhibit considerable sensitivity at room temperature to low concentration of NO_2 (4 ppm) during response time up to 45 s.

Keywords:

Nano-Porous silicon, Macro-porous silicon, stain-etching, NO_2 detection, room temperature

1. Introduction

Several materials with large specific surface areas, such as polymer membranes [1], carbon nanotubes [2], and metal oxides [3-5] have been studied as prospective candidates for future gas sensors. Actually, the most used gas sensors are based on metal oxides whose principle is based generally on chemisorption interactions which are oxydo-reduction reactions based on the exchange of electrons between the gas and the sensitive layer. The reactions take place on the surface on specific adsorption sites thermodynamically favorable. These reactions depend on the gas type and adsorption sites. It has been shown that oxygen is necessary to catalyze the sensing reaction in which the gas reacts generally with the adsorbed oxygen molecules. Currently, in the most developed sensors, the sensitive layer is nanostructured, which considerably increases the number of adsorption sites. In this work, one way of improvement consists of increasing the sensor specific surface which can be achieved by using a porous silicon substrate. Porous silicon (PS), an interesting material with large specific surface area, is easily produced by chemical [6, 7] or electrochemical [8] processes. It is indeed a very variable material who's optical, electrical and morphological properties could be modulated by porosity and thickness. It presents a high specific surface up to 1500 m^2/cm^{-3}. Chemical functionalization of the porous silicon surface shows the potential for developing a variety of gas sensors [6]. Recently, PS gas sensor has been investigated especially for NO_2 detection [9, 10]. Although PS sensors show good sensitivity when exposed to NO_2, some problems such as selectivity, repeatability, response–recovery characteristics and long-term stability need to be considered. In the literature, some research works have reported incomplete recovery, and irreversible behaviors limiting the PS integration in final gas-sensing devices [11, 12]. In addition, the use of multilayer structures with different morphologies based on porous silicon (different pore sizes, porosity) obtained on the same substrate has been investigated for NO_2 gas sensor [13]. In other reports, porous silicon membranes are investigated in gas sensors using hybrid and composite materials leading to the selectivity enhancement [13]. The PS with ordered pore channels may influence considerably the gas-sensing properties, including reversibility and response–recovery time. Moreover, porous silicon sensing properties could be ameliorated by catalyst deposition and modifying PS surface [14].

However, the porous silicon presents unstable Si-H bonds on its surface which are rapidly degraded under ambient conditions leading to surface oxidation and therefore the interface states and dangling bonds presence. The formation of SiO_x layer is certainly playing an important role on gas detection.

In this work, we present an original study focused on the use of two different types of porous silicon (PS) obtained by a simple and low-cost method as a gas senor at room temperature: nano-porous silicon (nano-PS) and macro-porous silicon (macro-PS). The PS gas sensing properties and response/recovery characteristics at room temperature are investigated and discussed.

2. Experimental details

2.1 Samples preparation :

Nano porous (nano-PS) and macro porous (macro-PS) silicon samples were synthesized via stain etching technique during 2 min using etching solution (HF, HNO_3, H_2O) = (1, 2, 3) in volumetric ratio (Fig.1(a)). P-type and N-type silicon substrates with a resistivity of~ 1-3 Ω.cm and a thickness of 200 µm were used to elaborate nano-PS and macro-PS samples respectively. To elaborate macro-PS samples, light is used during the etching process in order to create holes necessary for the etching process.

Before PS elaboration, the substrates have followed different cleaning steps to eliminate organic greases by immerging samples in boiling acetone during 10 min then in ethanol during 5 min and deionized water. Finally, the native oxide was etched in 10 % acid hydrofluoric during 1 min, rinsed in deionized water and dried with nitrogen. After porous silicon formation, aluminum (Al) electrodes are deposited on PS surface by thermal evaporation with a thickness of about 100 nm in a parallel configuration.

2.2 Physicochemical samples characterization:

The formed porous silicon was studied using a Fourier Transform Infrared (FTIR) Nicolet MAGNA-IR 560 Spectrometer. The PS morphology was investigated by a scanning electron microscope (SEM). The elemental analysis of PS surface was performed by the X-ray Dispersive Energy (EDX) coupled with SEM. Effective minority carrier lifetime (τ_{eff}) was studied using a microwave induced photoconductive decay technique (μW-PCD). The measurements are performed by Semilab WT-2000 system using a 904 nm laser excitation source.

2.3 Gas sensing measurement:

The gas-sensing performances of the PS sensors were tested in a dynamic gas sensing testing system, as shown in Fig.1 (b). The sensor was placed on a heating plate connected to a temperature controller to adjust the operating temperature. By measuring the resistance change over time between two electrodes under gas, the sensor dynamic response curves were collected. In this work, the gas sensor response is defined as:

R_a/R_g (When sensor is exposed to an oxidizing gas) (Eq. 1-a)

Or R_g/R_a (When sensor is exposed to a reducing gas) (Eq. 1-b)

Where R_a and R_g are the sensor resistances measured in dry air and under tested gas, respectively. The PS sensors are tested toward exposed gas at room temperature (RT) (25 ± 2 °C). The response and recovery times are also calculated. The response time is measured as the time necessary for the resistance to reach 90 % of the equilibrium value after gas exposure. The recovery time is obtained as the time required reaching 10 % above initial resistance after gas removal. The samples were exposed to different gas as NO_2, NH_3, O_3 and CO. Ozone is generated from dry air, using a system based on a UV lamp. The dry air passes through a quartz tube illuminated by the UV lamp. Exposure of oxygen molecules to UV rays leads to the generation of ozone molecules.

3. Results and discussion:

3.1. Porous silicon characterization:

For silicon nanostructuring, there are two possible approaches: the top-down and the bottom-up approaches. In this work, porous silicon is obtained by the top-Down approach consisting in miniaturizing the silicon substrate until obtaining nanometric structures by etching the initial substrate in an acidic solution. The stain-etching process is composed of two chemical reactions occurring simultaneously: the silicon surface oxidation by the nitric acid and the silicon oxide etching by hydrofluoric acid. Porous silicon is characterized by the morphology, the porosity and the thickness. Porosity is defined as the fraction of voids within the porous structure [16]. The quantification of the material loss in the etching process is used as a gravimetric measurement to evaluate the PS porosity and thickness [17]. The following equations are used to obtain the average porosity (P) (Eq. 2).

$$P = \frac{m_1 - m_2}{m_1 - m_3} \qquad \text{(Eq. 2)}$$

The sample was weighted before porosification (m_1), after porosification (m_2), and after porous silicon dissolution in 1 wt.% NaOH solution (m_3). ρ is the density of silicon and S is the etched area. The porosity of the elaborated porous silicon is about 38% and 66 % for nano-PS and macro-PS respectively. Fig. 2 shows the nano-PS surface morphology obtained by SEM microscopy. The top surface SEM images (Fig. 2(a-b)) shows the presence of pores with nanometric sizes less than 10 nm confirming the synthesis of nano porous structure. The PS layer thickness estimated thanks to the cross-section SEM image (Fig. 2(c)) is about 0.64 µm. Fig. 3(a-b) shows the macro-PS surface morphology. We distinguish the presence of pores with sizes more than 50 nm proving the formation of macro-porous silicon layer with a thickness of 1.6 µm (Fig. 3(c)). The X-ray Dispersive Energy (EDX) coupled to the SEM performed on the nano-PS porous silicon sample shows that no metallic impurities related to the synthesis method were detected (Fig. 2(d)). The presence of an oxygen peak indicates the surface oxidation. In fact, the hydrogenation via HF and the formation of Si-H bonds is only stable during low durations. Stored in ambient atmosphere, the Si-H bonds are rapidly degraded leading to the porous surface oxidation and therefore the presence of dangling bonds which could play an important role in gas sensing mechanism. In order to confirm this observation, FTIR spectra of freshly prepared and oxidized PS samples were performed (Fig.4) showing the vibration bands attributed to SiH_x and Si-O-Si stretching mode at 2112 cm^{-1} and 1092 cm^{-1} respectively, the SiH_2 scissors mode (907 cm^{-1}), the Si-Si stretching mode (628 cm^{-1}), SiH_n and O-SiH_x wagging mode at 672.7 cm^{-1} 861 cm^{-1} respectively[18]. Comparing the two spectra, we notice the reduction of the SiH_x peak at 2112 cm^{-1} against the increase in Si-O peak intensity confirming the PS surface oxidation.

Fig. 5 presents the 2D mapping image and the corresponding histogram with 250 µm resolution showing the minority carrier lifetime in p-silicon substrate (Fig. 5(a)), nano-PS sample (Fig. 5(b)), n-silicon substarte (Fig. 5(c)) and macro-PS sample (Fig. 5(d)). As we can notice, the lifetime in freshly prepared nano-PS layer is homogeneous and greater than that in silicon thanks to the surface hydrogenation during the etching process in HF/HNO_3 solution. For the macro-PS sample, a slight enhancement in τ_{eff} is also obtained. We note also that the average τ_{eff} measured in the macro-PS (13µs) is greater than that of the nano-PS sample (1.9 µs) attributed to the quality of the initial silicon substrate used.

3.2 Gas sensing properties:

The gas sensing properties of the nano-PS and macro-PS sensors towards 4 ppm of NO_2 gas were studied at room temperature in dry air. Fig. 6(a) shows the variation of the electrical resistance as a function of time with a temperature increasing from 25 to 50 °C. The results show that the resistance decreases with increasing the temperature proving the semiconductor behavior of the PS sensor. The nano-PS gas sensor response as a function of time at room temperature is shown in Fig.6 (b). This sensor has a response about 1.5 at ambient temperature, as well as reasonable response (45 s) and recovery times (67 s). The gas sensor based on nano-PS is therefore operational in ambient temperature. The recovery time is considered interesting thanks to the low thickness of the PS layer (about 640 nm).

Fig.6 (c) shows the good repeatability of the nano-PS sensor for three dynamic response cycles for an exposure time of 1 min and for two dynamic cycles for an exposure time of 3 min. For each test, complete recovery of initial resistance is observed. This indicates that porous silicon has a chemical stability when it comes to NO_2, the gas particles are able to be adsorbed, and then desorbed rapidly at room temperature once the experiment is over. The gas selectivity of porous silicon sensors is also studied. Fig. 6(d) shows the sensor response under

different gas (4 ppm NO_2, 4 ppm NH_3, 200 ppb O_3 and 4 ppm CO) at room temperature. As noted, the best response is recorded to NO_2 however the sensor response towards NH_3 and O_3 is very low. When exposed to CO, the sensor does not display any sensitivity. The CO gas is still presenting problems of detection as few research works have reported on CO sensing in particular at room temperature. These results show that NO_2 is the most compatible gas for this sensor. Table 2 recapitulates the different characteristics of the nano-PS sensor. For the different detected gas, the nano-PS sensor exhibits a rapid response proving its efficiency while the highest recovery time is obtained when it is exposed to NH_3.

The gas sensing properties of the macro-PS sensors towards 4 ppm of NO_2 gas were studied at room temperature. Fig. 7 shows the macro-PS gas sensor response as a function of time. The sensor had a response of 2.35 at room temperature, much higher than nano-PS sensor response. The response and recovery times of this sensor were determinated and the values were about 64 s and 45 min, respectively. This sensor shows a very slow recovery characteristic attributed to the high thickness of the PS layer (about 1.6 µm). The selectivity of macro-porous silicon sensors is also studied. Fig. 7(b) shows the sensor response under different gas (4 ppm NO_2, 4 ppm NH_3, 200 ppb O_3 and 4 ppm CO) at room temperature. The macro-PS sensor exhibited the important gas sensing characteristic for NO_2 gas. Table 3 recapitulates the different characteristics of the macro-PS sensor. We can consider that NO2 gas is the most compatible gas for this sensor.

Compared to the nano-PS sensor results, the increase in sensitivity for the macro-PS sensor is attributed to the obtained morphology (Fig.2 and Fig.3). The nano-PS presents nano-sized pores less than 10 nm however the macro-PS has macro-pores. Besides, the macro-PS sample has a higher porosity justifying that a higher quantity of gas molecules is adsorbed in the macro-PS than in the nano-PS sensor. Comparing the recovery times measured for the two sensors, we note that the gas desorption takes much more time with macro-PS sensor attributed to the porous layer thickness (1.6 µm for macro-PS against 0.64 µm for the nano-PS).

3.3 Sensing mechanism:

The response of most gas sensors is due to the changes in carrier concentration, usually induced by adsorption-desorption reactions on the sensing materials surface. In recent years, many researchers have investigated the NO_2-sensing mechanism of porous silicon [20, 21]. It is found that the PS belongs to the surface-controlled type as both surface states and oxygen adsorption play important roles in the NO_2 detection [22]. NO_2 acts as an oxidizing gas, which will capture the electrons from the sensing material. In the first step, the atmospheric oxygen molecules, adsorbed onto the PS surface in the form of O^- and O_2^- depending on the operational temperature, are extracting electrons from the PS conduction band ((Eq. 7)-(Eq. 9)). In the case of the n-type porous silicon sensor, it leads to the formation of electron-depleted space-charge layer under the PS surface [23], and then the resistance increase.

$$O_2(gas) \rightarrow O_2(ads) \quad \text{(Eq. 7)}$$

$$O_2(ads) + é \rightarrow O_2^-(ads), \; T<100\ °C \quad \text{(Eq. 8)}$$

$$O_2^-(ads) + é \rightarrow 2O^-(ads), \; 100\ °C<T<300\ °C \quad \text{(Eq. 9)}$$

In the second step, when the PS sensor is exposed to NO_2, the gas molecules may be directly adsorbed onto the PS surface by trapping electrons (Eq. 10), and interact with the chemisorbed oxygen (such as O^- and O_2^-) ((Eq. 11) and (Eq. 12)) [24].

$NO_2\,(gas) + é \rightarrow NO_2^-(ads)$ (Eq. 10)

$NO_2\,(gas) + O_2^-(ads) + 2é \rightarrow NO_2^-(ads) + 2O^-\,(ads)$, T<100 °C (Eq. 11)

$NO_2\,(gas) + O^-(ads) + 2é \rightarrow NO_2^-(ads) + O^{2-}\,(ads)$, 100 °C<T<300 °C (Eq. 12)

The reaction with NO_2 will increase further the electron depletion layer width and potential barriers, and then increase the sensor resistance [25]. Consequently, NO_2 molecules capture the electrons from PS surface, leading to the decrease of free electron concentration [26] leading to the sensor resistance increase. The PS electrical conductivity is significantly modulated depending upon the presence or the absence of NO_2, explaining the resistance variations. Fig. 8 presents the NO_2-sensing mechanism diagram of the n-type porous silicon at room temperature. Initially, the sensing material presents a flat band structure (Fig 8 (a)). At room temperature, the oxygen molecules are chemisorbed in the form of O_2^- , leading to the formation of a depletion layer (Fig. 8(b)). This formed layer would be raised as a result of NO_2 gas molecules interaction with the chemisorbed oxygen (Fig. 8 (c)).

However, when n-type PS is exposed to a reducing gas (electron donor) such as ammonia (NH_3), the gas molecules adsorbed on the surface are interacting with the chemisorbed oxygen molecules. This reaction leads to the release of electrons trapped in the surface of oxygen and their injection into the porous silicon conduction band [27]. Thereby, the PS resistivity is decreasing. The same explanation could be conducted with p-type porous silicon.

4 Conclusion :

In summary, two types of porous silicon (nano-PS and macro-PS) were prepared for NO_2 detection through simple chemical method. It was found that the prepared PS is promising for low-concentration NO_2 sensing at room temperature. Using the same technique and synthesis parameters, the two prepared sensors exhibit different behaviors. The substrate doping, and accordingly the obtained morphology, should be accounted for the PS gas sensors. In this study, we obtained responses towards low concentration of NO_2 at room temperature so the operational temperature is no longer an issue when using porous silicon as a sensing material. Therefore with porous silicon, the heater is no longer an essential component of the system.

Acknowledgements:

This work was supported by the bilateral Tuniso-French PHC-UTIQUE project (Code CMCU: 20G1108-Code Campus France: 44146SM).
The authors wish to thank Damien Chaudanson and Alexandre Altié for SEM measurements done at the Centre Interdisciplinaire de Nanoscience de Marseille (CINaM).

Conflict of Interest Statement:

The authors declare that they have no conflict of interest.

References

[1] H. Bai and G. Shi, Gas Sensors Based on Conducting Polymers. Sensors. **7**, 267 (2007).

[2] P. Slobodian, P. Riha, A. Lengalova, P. Svoboda, P. Saha, Multi-wall carbon nanotube networks as potential resistive gas sensors for organic vapor detection, Carbon. **49**, 2499 (2011).

[3] B. Comert Sertel, N. Akin Sonmez, M. Donmez Kaya, S. Ozcelik, Development of MgO: TiO_2 thin films for gas sensor applications. Ceram. Int. **45**, 2917 (2019).

[4] R. Moraes Oliveira, M.S. Vieira, M.N.F. Silva, Enhancement of acetylene gas sensing properties for ZnO-based gas sensor produced by plasma immersion ion implantation and deposition. Mater. Sci. Semicond. Process. **93**, 339 (2019).

[5] M.S. Barbosa, P.H. Suman, J.J. Kim, H.L. Tuller, M.O. Orlandi, Investigation of electronic and chemical sensitization effects promoted by Pt and Pd nanoparticles on single-crystalline SnO nanobelt-based gas sensors. Sens. Actuators B. **301**, 127055 (2019)

[6] H. Mhamdi, R. B. Zaghouani, T. Fiorido, J.L. Lazzari, M. Bendahan, W. Dimassi; Study of n-WO_3/p-porous silicon structures for gas-sensing applications, Journal of Materials Science: Materials in Electronics. **31**, 7862 (2020).

[7] K. Azaiez, R. B. Zaghouani, S. Khamlich, H. Meddeb, W. Dimassi, Enhancement of porous silicon photoluminescence property by lithium chloride treatment, Applied Surface Science. **441**, 272 (2018).

[8] K. Azaiez, R. B. Zaghouani, M. Daoudi, M. Amlouk, W. Dimassi, Enhancement photoluminescence property of porous silicon treated with bismuth (III). Inorganic Chemistry Communications 130, 108679. (2021).

[9] C. Hui-Qing, H. Ming, Z. Jing, and W. Wei-Dan, The light-enhanced NO_2 sensing properties of porous silicon gas sensors at room temperature, Chin. Phys. **21** (2012).

[10] W. Bdaiwi, Fabrication of Gas Sensor Device for H_2 and NO_2 from Porous Silicon, Applied Physics Research. **7** (2015).

[11] Z. Gaburro, P. Bettotti, M. Saiani, L. Pavesi, L. Pancheri, C.J. Oton, N. Capuj, Role of microstructure in porous silicon gas sensor for NO_2, Applied Physics Letters. **85,** 555 (2004).

[12] E. Massera, I. Nasti, L. Quercia, I. Rea, G. Di Francia, Improvement of stability and recovery time inporous-silicon-based NO_2, sensor, Sensors and Actuators B. **102**, 195 (2004).

[13] V. V. Bolotov, K. E. Ivlev, E. V. Knyazev, I. V. Ponomareva, and V. E. Roslikov, Formation of Multilayer Structures with Integrated Membranes Based on Porous Silicon, Fizika I Tekhnika Poluprovodnikov. **54**, 504 (2020).

[14] V. E. Galstyan, K.S. Martirosyan, V.M. Aroutiounian, V.M Arakelyan, A.H. Arakelyan, P.G. Soukiassian, Investigations of hydrogen sensors made of porous silicon, Thin Solid Films.517, 239 (2008).

[16] X. Yang, H. Beyenal, G. Harkin, Z. Lewandowski, Quantifying biofilm structure using image analysis, Journal of Microbiological Methods. **39**, 109 (2000).

[17] R. B. Zaghouani, M. Alaya, H. Nouri, J.-L. Lazzari, W. Dimassi, Study of WO3-decorated porous silicon and Al2O3-ALD encapsulation. Journal of Materials science:Materials in Electronics 29,17731 (2018).

[18] M. Alaya, R.B. Zaghouani, S. Khamlich, J.L. Lazzari, W. Dimassi, Enhancement of physical properties of stain-etched porous silicon by integration of WO_3 nanoparticles, Thin Solid Films **645**, 51 (2018).

[19] J. Diaz-Reyes, V. Dorantes-Garcia, A. Pérez-Benitez, J.A. Baderas-Lopez, Obtaining of films of tungsten trioxide (WO_3) by resistive heating of a tungsten filament. Superf. Vacio. **21**, 12 (2008).

[20] Z. Gaburro, C.J. Oton, L. Pavesi, Opposite effects of NO_2 on electrical injection in porous silicon gas sensors, Applied Physics Letters. **84**, 4388 (2004).

[21] L. Boarino, M. Rocchia, C. Baratto, A.M. Rossi, E. Garrone, S. Borini, F. Geobaldo, E. Comini, G. Faglia, G. Sberveglieri, G. Amato, Towards a deeper comprehension of the interaction mechanisms between mesoporous silicon and NO_2, Physica Status Solidi A. **182**, 465 (2000).

[22] P. Sun, M. Hu, M.D. Li, S.Y. Ma, Microstructure, electrical and gas sensing properties of meso-porous silicon and macro-porous silicon, Acta Physico-Chimica Sinica. **28**, 489 (2012).

[23] N.K. Ali, M.R. Hashim, A.A. Aziz, Effects of surface passivation in porous silicon as H_2 gas sensor, Solid-State Electronics. **52**, 1071 (2008).

[24] C.M. Ghimbeu, J. Schoonman, M. Lumbreras, M. Siadat, Electrostatic spray deposited zinc oxide films for gas sensor applications, Applied Surface Science. **253**, 7483 (2007).

[25] D. Stievenard, D. Deresmes, Are electrical properties of an aluminium-porous silicon junction governed by dangling bonds, Applied Physics Letters. **67**, 1570 (1995).

[26] E.A. Konstantinova, L.A. Osminkina, C.S. Sharov, V.Yu. Timoshenko, P.K. Kashkarov, Influence of NO_2 molecule adsorption on free charge carriers and spin centers in porous silicon, Physica Status Solidi A. **202**, 1592 (2005).

[27] G. H. Mhlongo, D. E. Motaung, F. R. Cummings, H. C. Swart, S. S. Ray, A highly responsive NH_3 sensor based on Pd-loaded ZnO nanoparticles prepared via a chemical precipitation approach, Scientific reports 9, 9881(2019).

Figure Caption

Figure 1: (a) Schematic illustration of the adopted porous silicon synthesis process. (b) The schematic diagram of the static gas-sensing test system.

Figure 2: SEM images of nano-PS sample: (a-b) top surface and (c): cross section images (d) EDX diagram of porous silicon.

Figure 3: SEM images of macro-PS sample: (a-b) top surface and (c): cross section images.

Figure 4: FTIR absorption spectrum of porous silicon PS sample.

Figure 5: The 2D mapping image of the minority carrier lifetime in (a) p-silicon, (b) Nano-porous silicon (nano-PS), (c) n-silicon and (d) Macro-porous silicon (macro-PS).

Figure 6: (a) Resistance variation of nano-PS as a function of time under dry air with simultaneous increase of temperature from 25 °C to 50 °C (b) Dynamic response and (c) Resistance variation of the nano-PS sensor exposed to 4 ppm of NO_2 (d) Selectivity towards NO_2, NH_3, O_3 and CO at room temperature.

Figure 7: (a) Dynamic response of macro-PS as a function of time under dry air, (b) Selectivity of macro-PS towards NO_2, NH_3, O_3 and CO at room temperature.

Figure 8: The schematic NO_2-sensing mechanism of n-type porous silicon.

Table

Table 1: Comparative of morphological and electronic parameters of nano-PS and macro-PS samples.

Table 2: The gas sensing properties of the nano-PS sensor towards different gases at room temperature.

Table 3: The gas sensing properties of the macro-PS sensor towards different gases at room temperature.

Table 1

	Porosity	Thichness of PS layer	Carrier lifetime
Nano-PS	38 %	0.64 µm	1.9 µs
Macro-PS	66%	1.6 µm	13 µs

Table 2

Gas	NO_2	NH_3	O_3	CO
Gas concentration	4 ppm	4 ppm	200 ppb	4 ppm
Sensibility	1.50	1.06	1.10	No response
Response time	45 s	70 s	58 s	//
Recovery time	67 s	960 s	240 s	//

Table 3

Gas	NO_2	NH_3	O_3	CO
Gas concentration	4 ppm	4 ppm	200 ppb	4 ppm
Sensibility	2.35	1.10	1.08	No response
Response time	64 s	80 s	60 s	//
Recovery time	45 min	180 min	45 min	//

Figure 1

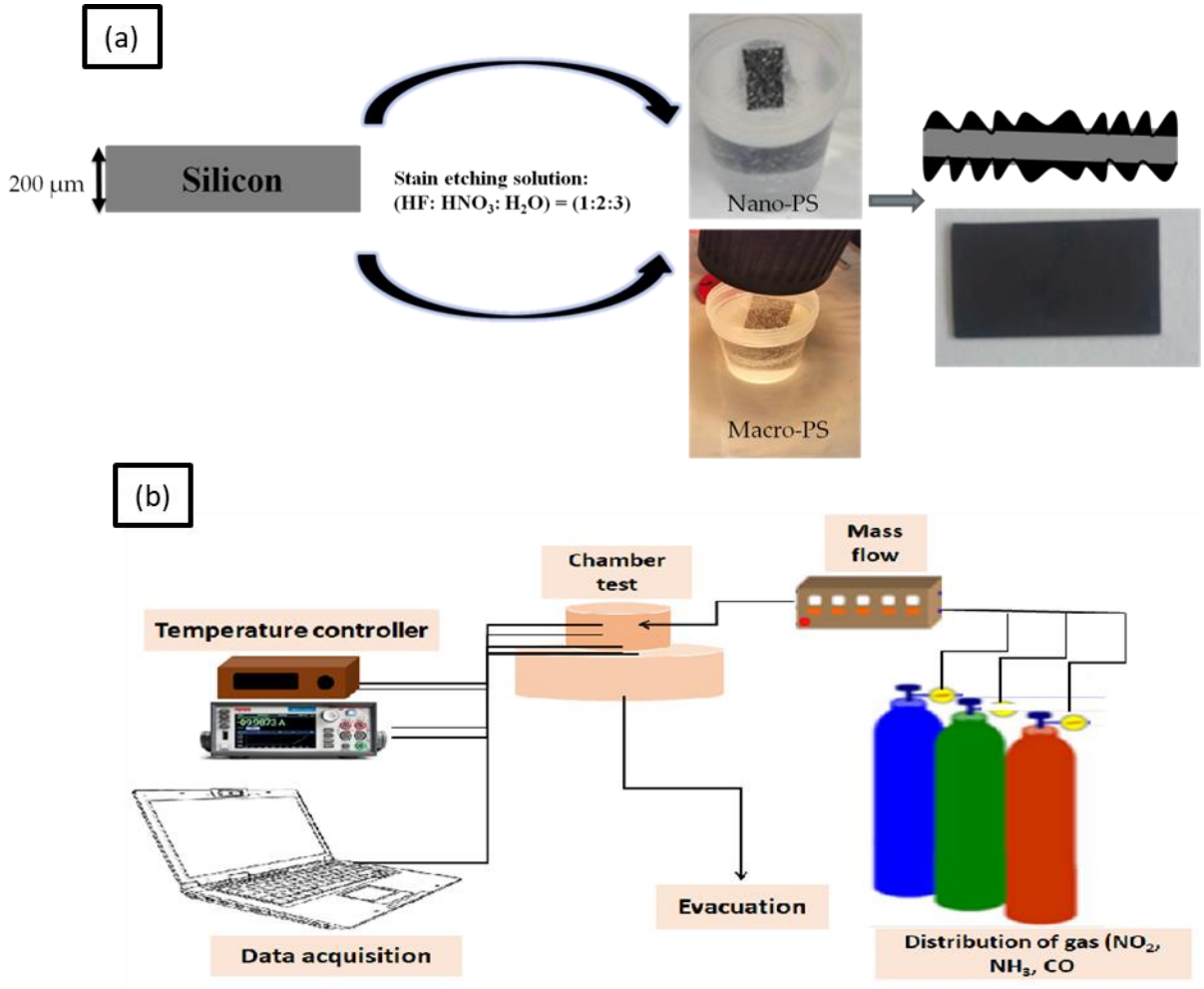
(a)
200 µm
Silicon
Stain etching solution:
(HF: HNO3: H2O) = (1:2:3)
Nano-PS
Macro-PS
(b)
Mass flow
Chamber test
Temperature controller
Evacuation
Data acquisition
Distribution of gas (NO2, NH3, CO

Figure 2

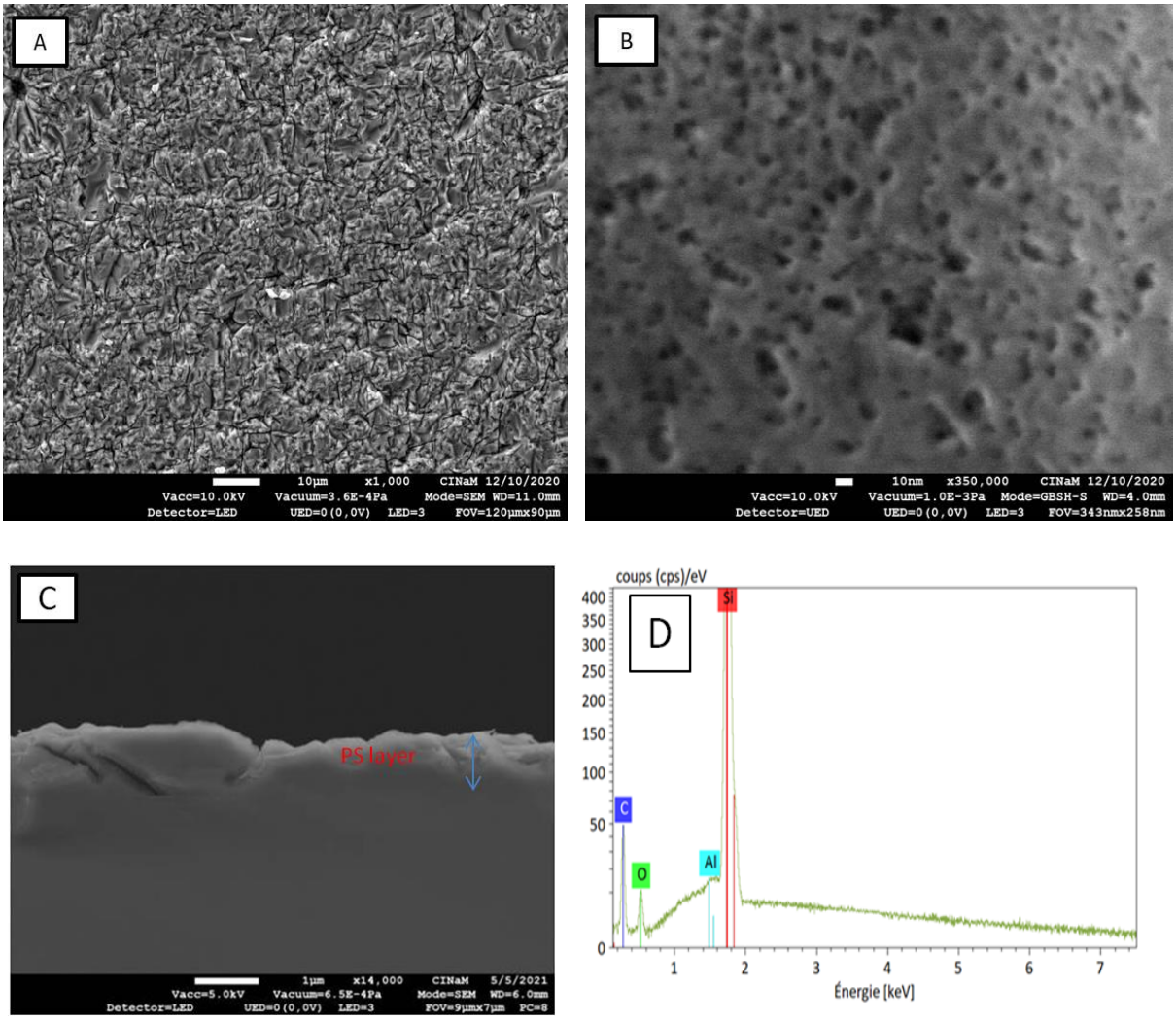
A
10µm x1,000 CINaM 12/10/2020
Vacc=10.0kV Vacuum=3.6E-4Pa Mode=SEM WD=11.0mm
Detector=LED UED=0(0,0V) LED=3 FOV=120µmx90µm
B
10nm x350,000 CINaM 12/10/2020
Vacc=10.0kV Vacuum=1.0E-3Pa Mode=GBSH-S WD=4.0mm
Detector=UED UED=0(0,0V) LED=3 FOV=343nmx258nm
C
PS layer
1µm x14,000 CINaM 5/5/2021
Vacc=5.0kV Vacuum=6.5E-4Pa Mode=SEM WD=6.0mm
Detector=LED UED=0(0,0V) LED=3 FOV=9µmx7µm PC=8
D
coups (cps)/eV
400
350
300
250
200
150
100
50
0
Si
C
O
Al
1
2
3
4
5
6
7
Énergie [keV]

Figure 3

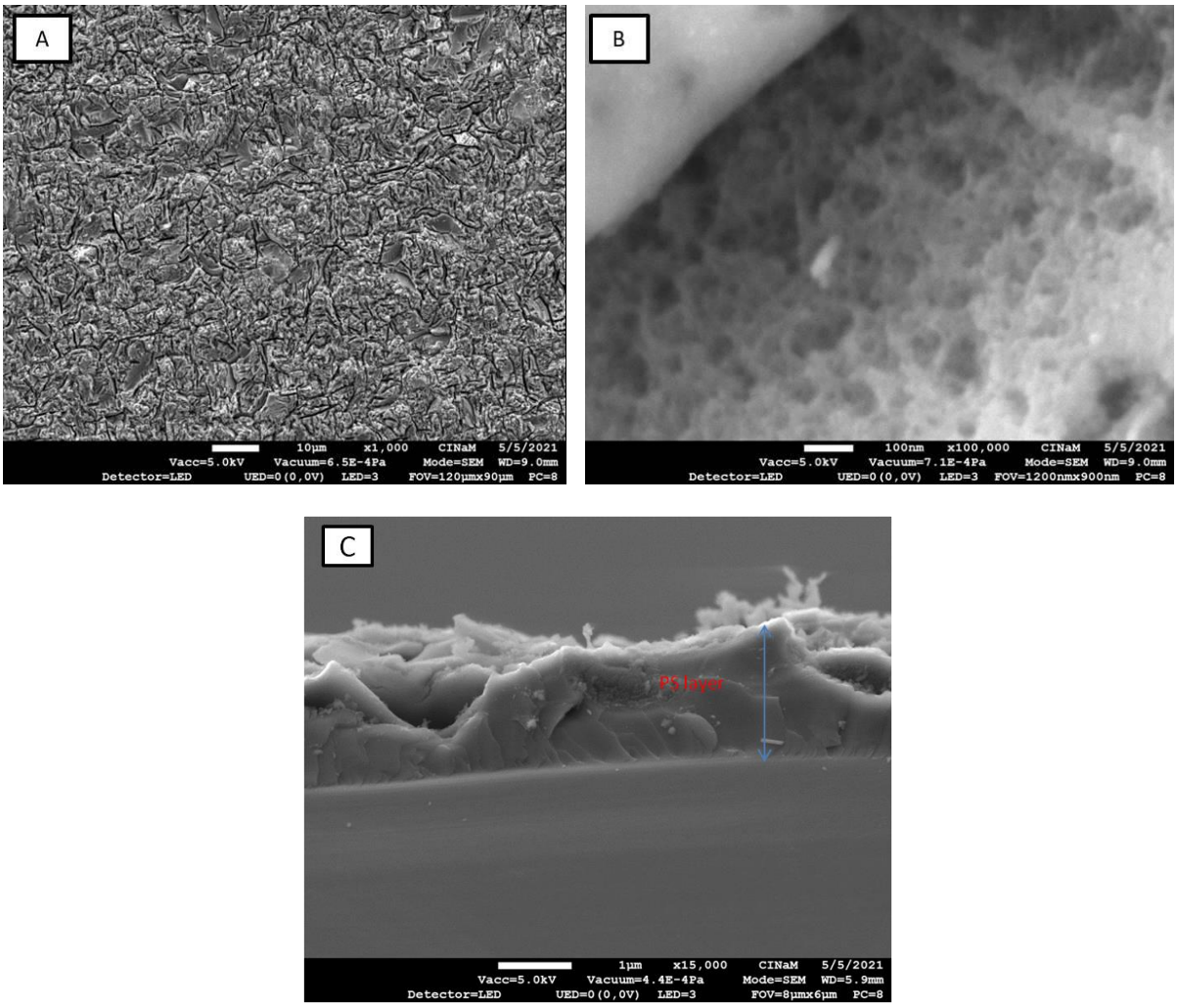
A
10µm x1,000 CINaM 5/5/2021
Vacc=5.0kV Vacuum=6.5E-4Pa Mode=SEM WD=9.0mm
Detector=LED UED=0(0,0V) LED=3 FOV=120µmx90µm PC=8
B
100nm x100,000 CINaM 5/5/2021
Vacc=5.0kV Vacuum=7.1E-4Pa Mode=SEM WD=9.0mm
Detector=LED UED=0(0,0V) LED=3 FOV=1200nmx900nm PC=8
C
PS layer
1µm x15,000 CINaM 5/5/2021
Vacc=5.0kV Vacuum=4.4E-4Pa Mode=SEM WD=5.9mm
Detector=LED UED=0(0,0V) LED=3 FOV=8µmx6µm PC=8

Figure 4

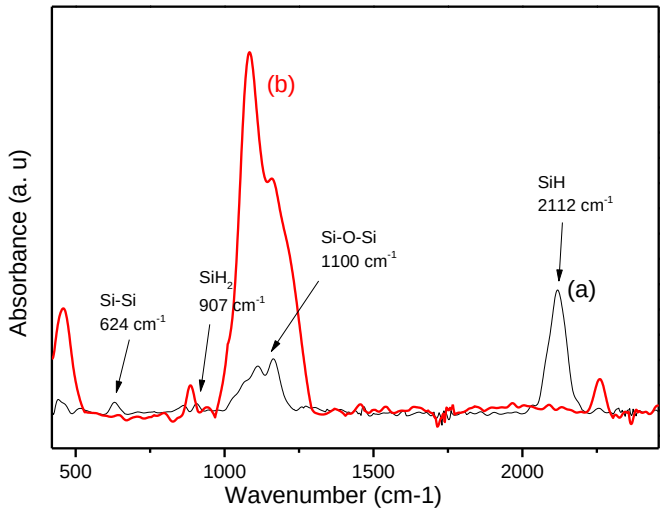
(b)
(a)
Si-Si
624 cm-1
SiH2
907 cm-1
Si-O-Si
1100 cm-1
SiH
2112 cm-1
Absorbance (a. u)
500
1000
1500
2000
Wavenumber (cm-1)

Figure 5

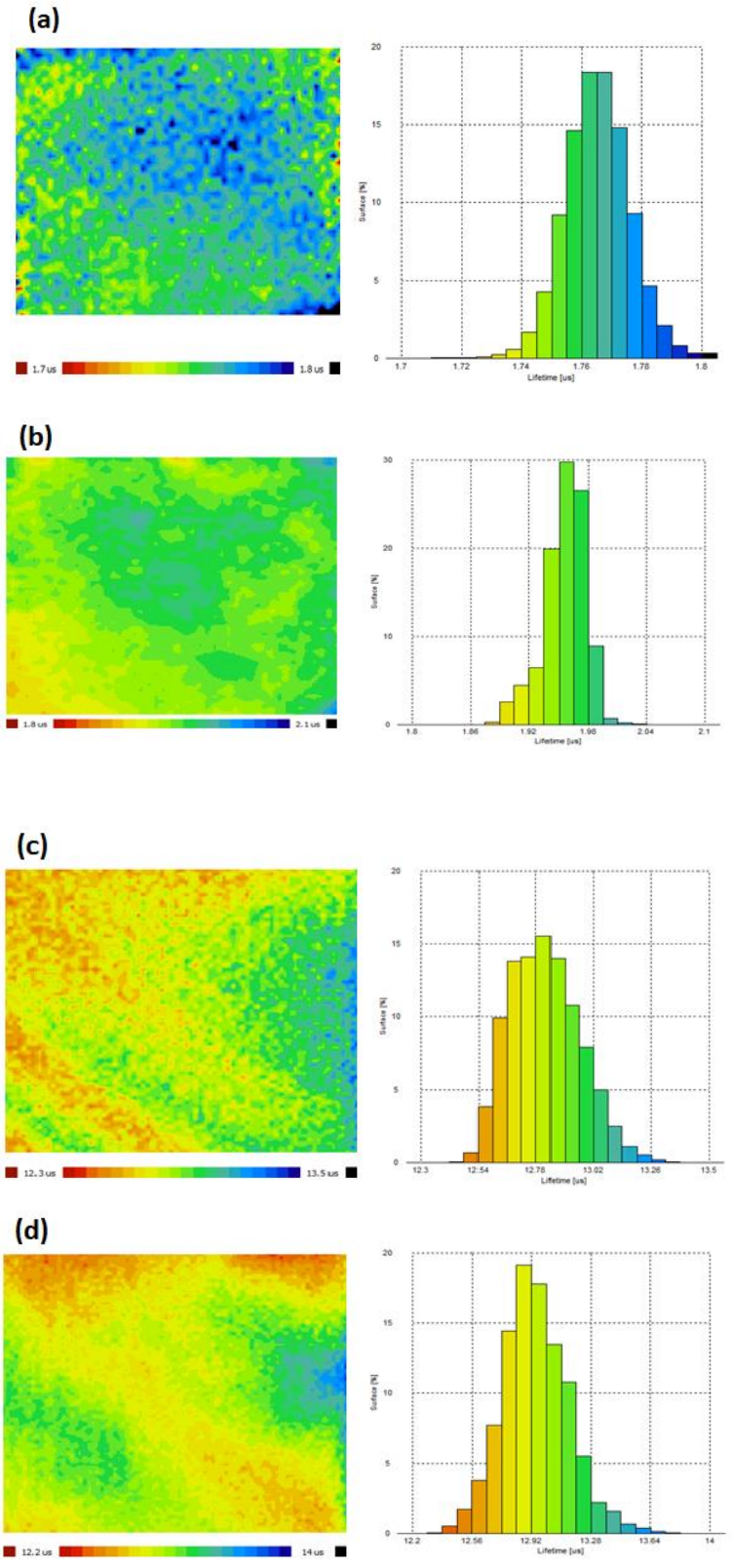
(a)
1.7 us
1.8 us
Surface [%]
Lifetime [us]
(b)
1.8 us
2.1 us
Surface [%]
Lifetime [us]
(c)
12.3 us
13.5 us
Surface [%]
Lifetime [us]
(d)
12.2 us
14 us
Surface [%]
Lifetime [us]

Figure 6(a)

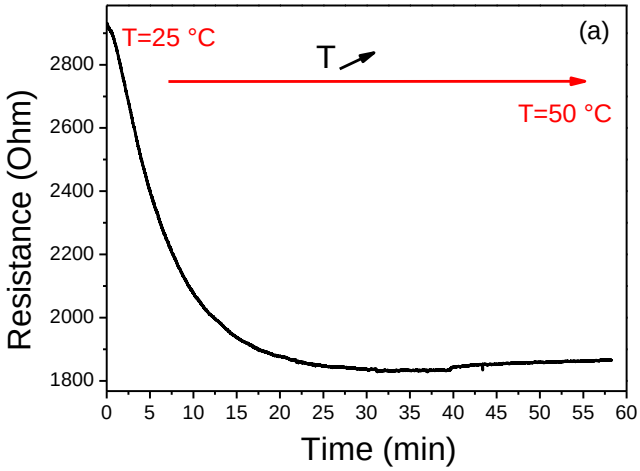

Figure 6(b)

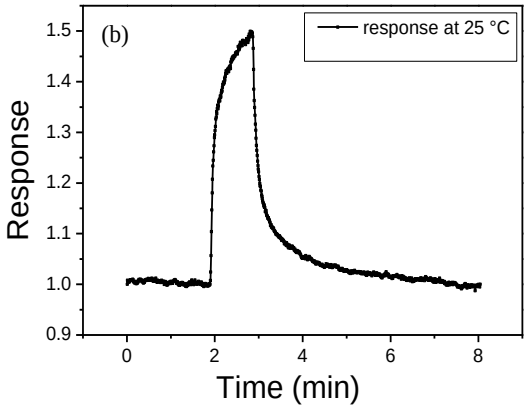

Figure 6(c)

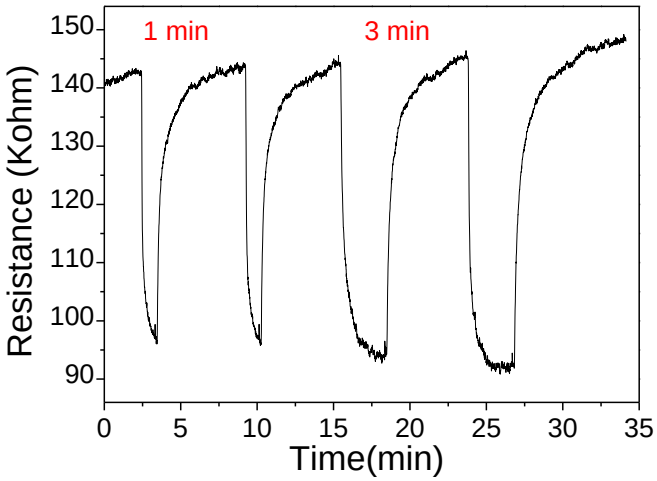

Figure 6 (d)

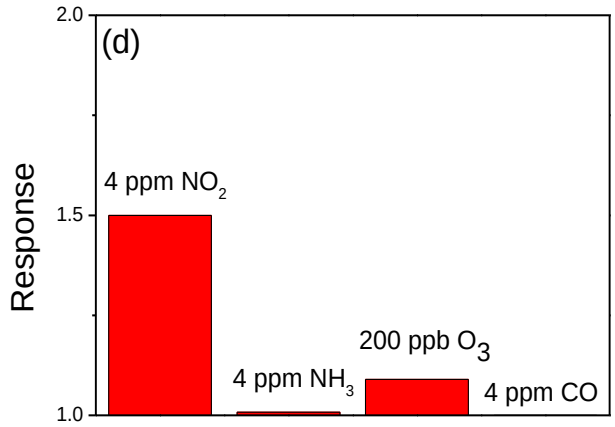

Figure 7(a)

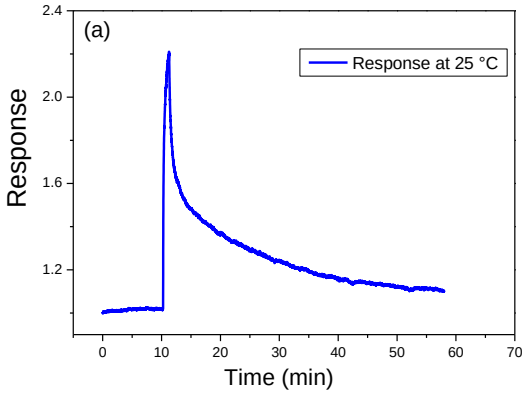

Figure 7(b)

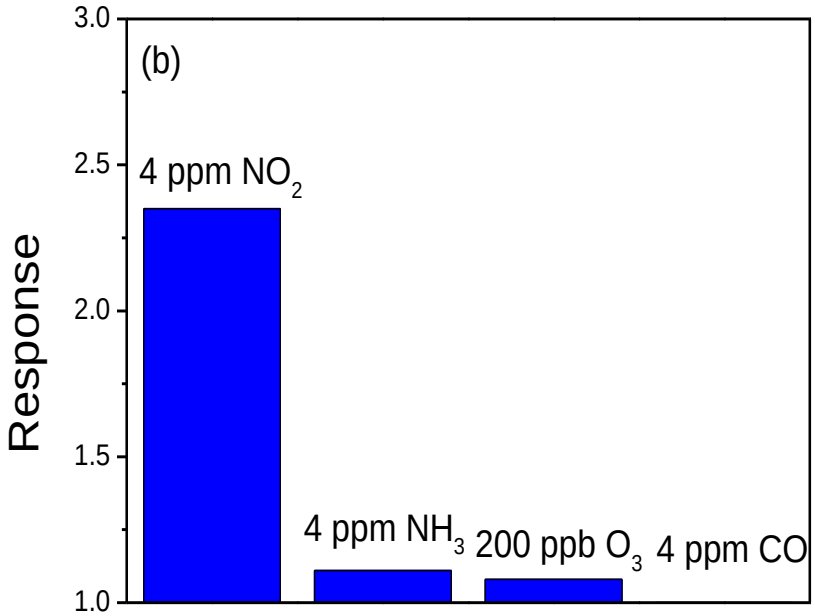

Figure 8

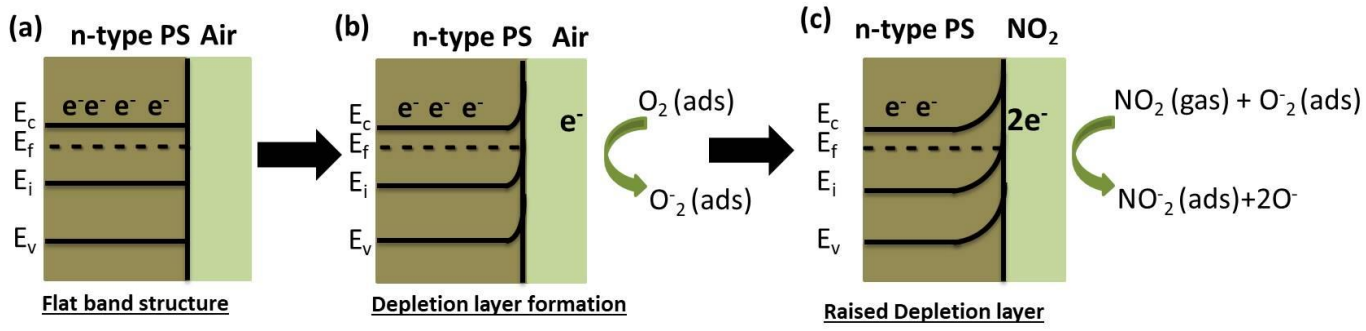
(a)
n-type PS Air
e⁻e⁻ e⁻ e⁻
E_c
E_f
E_i
E_v
Flat band structure
(b)
n-type PS Air
e⁻ e⁻ e⁻
e⁻
O₂ (ads)
O⁻₂ (ads)
Depletion layer formation
(c)
n-type PS NO₂
e⁻ e⁻
2e⁻
NO₂ (gas) + O⁻₂ (ads)
NO⁻₂ (ads)+2O⁻
Raised Depletion layer